

Coherent Plasma-Curvature Radiation in FRB

J. I. Katz,^{1*}

¹*Department of Physics and McDonnell Center for the Space Sciences, Washington University, St. Louis, Mo. 63130 USA*

7 September 2018

ABSTRACT

Curvature radiation is a natural candidate for the emission mechanism of FRB. However, FRB spectra have structure with $\Delta\nu/\nu \sim 0.03\text{--}0.2$, inconsistent with the very smooth spectrum of curvature radiation. Although this spectral structure might be attributed to chromatic scintillation or lensing, in four FRB high spectral resolution data indicate scintillation decorrelation bandwidths much narrower than the observed $\sim 30\text{--}300$ MHz spectral structure. Some of the observed structure may be intrinsic to the radiation mechanism. I suggest that the observed spectral structure reflects the spatial structure of a clumpy radiating charge distribution, and that the characteristic curvature radiation frequency may be higher than the observed frequencies. In this coupled plasma-curvature radiation process the radiated spectra are the product of the spectra of the plasma wave and that of incoherent curvature radiation. The argument applies to all coherent radiation processes, including those that produce pulsar nanoshots. The implied FRB “clump” charges are large, and produce electrostatic potentials that suggest electron Lorentz factors $\gtrsim 10^2$. The result applies generally to coherently radiating sources.

Key words: radio continuum: transients, radiation mechanisms: non-thermal

1 INTRODUCTION

The short durations and high radiated energy of Fast Radio Bursts (FRB) point to neutron stars, with their small size and deep gravitational potential wells, as their origin. The high brightness of FRB requires coherent radiation by “clumps” with net charges of multiple Coulombs (Katz 2014, 2016). A magnetic field provides possible energy sources, including reconnection of magnetostatic fields and magnetic dipole radiation and particle acceleration powered, as in radio pulsars, by rotational energy. It enables the emission of radio-frequency curvature radiation. Plasma instability powered by counterstreaming electrons and positrons provides additional radiation mechanisms.

Coherent curvature radiation has been often suggested as the radiation mechanism of FRB (Dai, Wang, Wu *et al.* 2016; Gu *et al.* 2016; Wang *et al.* 2016; Ghisellini & Locatelli 2018; Katz 2017b; Yang & Zhang 2017) because in the intense fields of neutron star magnetospheres any energy of gyration about field lines is very quickly radiated as X-rays or gamma-rays, leaving the particles to follow the field lines. Melrose (2017) presents a general review of coherent radiation processes and Kumar, Lu & Bhattacharya (2017); Lu & Kumar (2018) present a very detailed investigation in the context of FRB.

The spectra of FRB at frequencies in the 1.2–1.5 GHz band and, in a few observations, at frequencies from 700 MHz to 8 GHz, contain structure on frequency scales $\sim 30\text{--}300$ MHz (Keane *et al.* 2012; Thornton *et al.* 2013; Burke-Spolaor & Bannister 2014; Spitler *et al.* 2014; Masui *et al.* 2015; Petroff *et al.* 2015; Ravi, Shannon & Jameson 2015; Ravi *et al.* 2016; Scholz *et al.* 2016; Spitler *et al.* 2016; Bannister *et al.* 2017; Chatterjee *et al.* 2017; Hardy *et al.* 2017; Law *et al.* 2017; Marcote *et al.* 2017; Oostrum *et al.* 2017; Petroff *et al.* 2017; Gajjar *et al.* 2018; Michilli *et al.* 2018). Spectral structure could not be seen in the discovery paper (Lorimer, *et al.* 2007) because the dynamic spectral data were saturated.

Cordes, Wasserman, Hessels *et al.* (2017) attribute the complex temporal (on $\sim 100\ \mu\text{s}$ time scales) and spectral structure of FRB (Ravi *et al.* 2016; Gajjar *et al.* 2018; Michilli *et al.* 2018) to chromatic lensing, but the observed structure does not closely resemble the predictions of their Figs. 6 and 7. In this paper I consider an alternative explanation, that these properties are intrinsic to the plasma emission mechanism.

This behavior is widespread. Pulsar nanoshots have analogous frequency structure with $\Delta\nu \sim 0.1\nu$ (Soglasnov *et al.* 2004; Hankins & Eilek 2007). These nanoshots are, scaled up by many orders of magnitude, a popular model for FRB.

These observed spectra are inconsistent with the spectra emitted by point charges traveling on curved paths at

* E-mail katz@wuphys.wustl.edu

constant speed (acceleration perpendicular to velocity), and hence with a straightforward interpretation as curvature or synchrotron radiation (Katz 2014). Such particles radiate very smooth spectra (Jackson 1999), with a gradual rolloff between a low frequency asymptote $F(\omega) \propto \omega^{1/3}$ that is a weak function of frequency and a high frequency asymptote $F(\omega) \propto \omega^{1/2} \exp(-\omega/\omega_c)$ that falls off rapidly with increasing frequency. The characteristic frequency $\omega_c = 3c\gamma^3/(2\rho)$, where γ is the particle's Lorentz factor (taken as constant) and ρ the radius of curvature of its path. The same expression applies to synchrotron radiation as to curvature radiation, except that for curvature radiation ρ is given by the magnetic field geometry while for synchrotron radiation it is given by the radius of the charge's circular or helical path.

Katz (2014) explained these observations by attributing the radiation to emission by plasma waves, modeling them as electric dipole radiators. In this paper I suggest a hybrid plasma-curvature radiation process that recognizes that FRB are likely produced in regions of intense and curved magnetic fields. This process resolves the disagreement between the observed structured FRB spectra and the theoretical spectrum of curvature radiation. I first consider, and argue against, the hypothesis that the frequency structure is the result of chromatic scintillation along the propagation path. I then discuss the effect of the spatial structure of coherently radiating charge densities on the emitted spectrum, and argue that plasma-curvature radiation may explain the observed properties of FRB. Ghisellini & Locatelli (2018) discuss the broad, rather than high resolution, frequency structure of coherent curvature radiation, involving considerations other than the plasma waves suggested here.

2 SCINTILLATION

Can the frequency structure of FRB spectra be attributed to scintillation? Strong scintillation produces a Rayleigh distribution of received energy in non-overlapping temporal or spectral intervals. Data from temporal intervals are less useful because scintillation is less readily distinguished from variation in the source emission power (although the chromaticity of plasma scintillation might enable this distinction and there is no reason to expect intrinsic variations in emitted power to follow a Rayleigh distribution) and because bursts may be resolved into only a few temporal bins. In addition, temporal resolutions have been $\gtrsim 0.03$ ms, making it impossible to set upper limits on scintillation bandwidths $\gtrsim 30$ kHz.

2.1 Narrow Band Spectral Structure

Spectrally resolved data are more useful. The scintillation decorrelation bandwidths of four FRB have been measured or bounded:

Masui *et al.* (2015) found a spectral decorrelation width of 1.2 ± 0.4 MHz in FRB 110523 that also has spectral structure on a scale of ~ 10 – 30 MHz (their Fig. 1) around a frequency of 800 MHz (*cf.* the Stokes *I* data in their Fig. 2 and the spectral autocorrelation function in their Extended Data Fig. 3).

Ravi *et al.* (2016) found a decorrelation width (possibly interpretable as an upper limit) of 100 ± 50 kHz for FRB

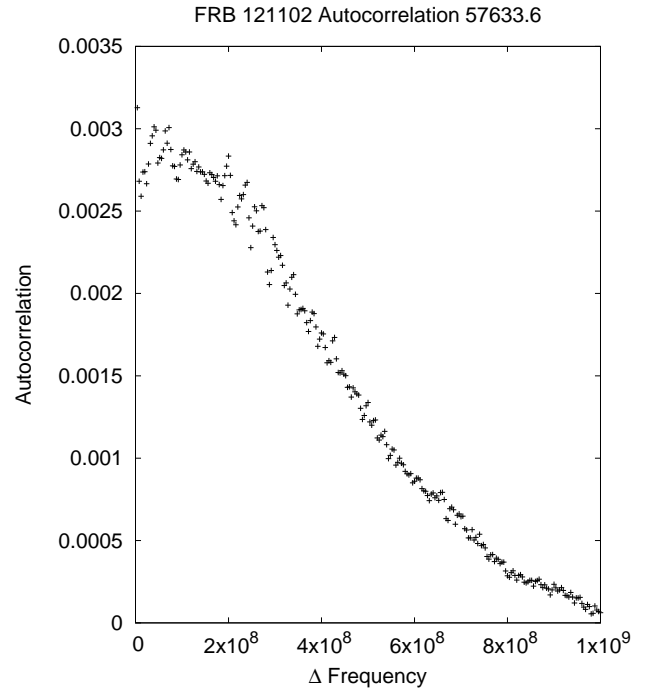


Figure 1. Spectral autocorrelation function of pulse 57633.6 from FRB 121102, observed at the VLA (Law *et al.* 2017). Normalization is arbitrary. The gradual rolloff reflects the ~ 250 MHz spectral width, while the absence of significant structure near the resolution of 4 MHz indicates a decorrelation width $\lesssim 4$ MHz.

150807. Fig. S9 of this paper shows a quantitative fit to a Rayleigh distribution, from which saturated scintillation may be inferred and the decorrelation bandwidth derived. This cannot itself explain the spectral structure evident on frequency scales of ~ 30 – 100 MHz. The spectro-temporal data in their Fig. 1 indicate that the frequency and temporal dependence on this frequency scale are not separable; with scintillation essentially constant through this sub-ms FRB, the spectral structure must be attributed to the emission mechanism.

The VLA observations (Law *et al.* 2017) of pulse 57633.6 (MJD 57633.67986367) of FRB 121102 around 3 GHz (their Fig. 4) suggest a Rayleigh distribution of energy, although a quantitative test is not possible because the underlying smooth spectral distribution is not known; their Gaussian is only a fit. Such a Rayleigh distribution would imply a decorrelation bandwidth less than the spectral resolution (4 MHz) of the data. The autocorrelation function is shown in Fig. 1 and indicates an upper bound on the decorrelation bandwidth of $\lesssim 4$ MHz. The expected Galactic scintillation bandwidth is ~ 7 MHz (Cordes & Lazio 2002; Law *et al.* 2017); if the full (including near-source contributions) scintillation bandwidth is < 4 MHz it explains the observed decorrelation.

Farah, Flynn, Bailes *et al.* (2018) found a spectra decorrelation width of about 1.5 MHz in FRB 170827 with substructure on scales of 100–200 kHz in UTMOST observations over a bandwidth of 31.25 MHz centered at 835 MHz. Although the observing bandwidth is narrow, compared to the Parkes bandwidth of 288 MHz centered at 1372.5 MHz

(Lorimer, *et al.* 2007), there appears to be structure on frequency scales broader than the 1.5 MHz decorrelation width.

2.2 Broad Band Spectral Structure

There is also spectral structure on broader scales of tens to hundreds of MHz. This is shown in “waterfall” plots for FRB 110220 (Thornton *et al.* 2013) and many other FRB (Petroff, Barr, Jameson *et al.* 2016), in Fig. 1 of Ravi *et al.* (2016) for FRB 150807, and and for FRB 121102 by Law *et al.* (2017); Michilli *et al.* (2018); Gajjar *et al.* (2018). Spitler *et al.* (2016) have argued that the varying spectral shapes of bursts from FRB 121102 are intrinsic, an argument I develop further here.

The broader frequency structure of FRB 121102 is difficult to explain as the result of scintillation. It varies greatly from burst to burst (Fig. 2 of Gajjar *et al.* (2018)) and even on sub-ms time scales within bursts (Gajjar *et al.* (2018) and Figs. 1 and ED1 of Michilli *et al.* (2018)). It is implausible that a scattering screen could change that rapidly (for Galactic pulsars the scintillation decorrelation time is minutes (Rickett 1990)), and in the nanoshots of the Crab pulsar the spectrum changes on $\sim \mu\text{s}$ time scales (Hankins & Eilek 2007), an even more demanding condition. If it were attributed to a slowly (compared to ~ 1 ms FRB durations) varying frequency-dependent scintillation pattern $f(\nu)$ then the complete spectro-temporal intensity function would be separable: $F(\nu, t) = f(\nu)g(t)$ with a temporal modulation $g(t)$, which is clearly not the case for FRB 121102 (Law *et al.* 2017; Michilli *et al.* 2018; Gajjar *et al.* 2018) although it may be valid for FRB 170827 (Farah, Flynn, Bailes *et al.* 2018). In addition, the distribution of intensities of this broad-band structure is unlike the Rayleigh statistics of strong scintillation that are observed (Fig. S9 of Ravi *et al.* (2016)) at frequency resolutions of a few MHz or less; Fig. 4 of Law *et al.* (2017) shows an excess of broad-band averaged intensities consistent, at high S/N , with zero that would be rare for Rayleigh statistics.

This broad frequency structure plausibly explained as rapid variation in the radiated spectrum. Such complex and rapidly changing spectra are very different from the smooth spectrum of accelerated point charges, either elementary charges or charges correlated in charge “bunches” that radiate as macro-point charges, and require explanation.

3 RADIATION BY A CONTINUOUS DISTRIBUTION OF CHARGE DENSITY

3.1 Spectrum

The radiation field produced by a charge moving at constant speed βc on a path locally approximated by a circular arc is a familiar classical result (Jackson 1999). Let $\theta(t_r) = \beta c t_r / \rho$ denote the position of the charge on the arc at the retarded time t_r , βc is the particle’s speed and ρ is the radius of curvature of the arc. The observer is at a distance d ($d \rightarrow \infty$) in a direction that makes an angle α to the plane of the osculating circular arc. Then the component of electric field perpendicular to the plane of the arc produced by a point

charge q is (Jackson 1999; Kumar, Lu & Bhattacharya 2017)

$$E_{point}(t_{obs}) = \frac{q\beta^2}{d\rho} \left[\frac{\cos\theta(t_r) - \beta \cos\alpha}{(1 - \beta \cos\theta(t_r) \cos\alpha)^3} \right], \quad (1)$$

where t_r is related to the observer’s time t_{obs} by

$$t_{obs} = t_r - \frac{\rho \cos\alpha}{c} \sin \frac{\beta c t_r}{\rho}. \quad (2)$$

This transcendental equation for $t_r(t_{obs})$ is readily solved numerically. $E_{point}(t_{obs})$ has the Fourier transform $E_{point,\omega}$, the familiar amplitude spectrum of radiation by an accelerated particle.

As calculated explicitly by Kumar, Lu & Bhattacharya (2017), this component of electric field has a non-zero mean (although it does change sign as the charge moves on its path), while the component in the plane of the orbit averages to zero. Both components have widths $\sim \rho/\gamma^3 c$, where $\gamma \gg 1$ is the particle’s Lorentz factor, corresponding to the characteristic frequency $\omega_c \sim \gamma^3 c/\rho$. Both components of field contribute to the radiation (that is strongly linearly polarized in this simple geometry), but it is sufficient to consider only one component.

Emission as bright as that of FRB requires enormous net charges radiating coherently (Katz 2014) and the incoherent emission of individual elementary charges (likely electrons and positrons) may be neglected. If there is a continuous distribution of net charge along the orbit $\lambda(\theta)$ each element of charge $dq = \lambda(\theta)d\theta$ contributes independently. The integral $\int dq$ must be small or zero (because otherwise a large electrostatic field would produce neutralizing currents) with near cancellation of regions of positive and negative charge; large local charge densities $|\lambda(\theta)|$ produce the intense radiation.

We assume that the charge density $\lambda(\theta)$ moves uniformly along the circular arc; λ is static in a frame moving at the speed βc and angular velocity $\beta c/\rho$. This assumption is not necessary, but leads to a simple result. The total electric field is found by integrating the contributions of each dq :

$$E_{tot}(t_{obs}) \propto \int E_{point}(t_{obs} - \Delta t) \lambda(\Delta\theta) d\Delta\theta \quad (3)$$

where $\Delta\theta = \beta c \Delta t / \rho$.

The spectrum of radiated power $P(\omega)$, is observed. By the Convolution Theorem

$$P(\omega) \propto |E_{tot,\omega}|^2 \propto |E_{point,\omega}|^2 |\lambda_\omega|^2. \quad (4)$$

$|E_{point,\omega}|^2$ is proportional to the familiar spectrum $F(\omega)$ of curvature or synchrotron radiation, increasing $\propto \omega^{1/3}$ for $\omega \ll c\gamma^3/\rho$ and falling nearly exponentially for $\omega > c\gamma^3/\rho$. λ_ω is the Fourier transform of $\lambda(\theta)$ with $\theta = \beta c \Delta t / \rho$. Eq. 4 relates the observed spectrum $P(\omega)$ to the charge density distribution λ_ω . The spatial scale of charge structure $\rho\theta \lesssim \gamma^3 \beta c / \omega$. The observation of spectral structure on a scale $\Delta\omega \ll \omega$ implies comparatively narrow-band spatial structure with a wave-number width $\Delta k \sim (\Delta\omega/\omega)k \sim \Delta\omega/(\gamma^3 \beta c)$.

For a point charge $\lambda(\theta) = q\delta(\theta - \theta_0)$, $\lambda_\omega = \text{Constant}$ and $P(\omega)$ is the usual spectrum of radiation by a single charge. For a uniform distribution of charge $\lambda(\theta) = \text{Constant}$, $\lambda_\omega \propto \delta(\omega)$ and there is only a stationary field, without radiation.

The charge density distribution, with power spectrum $|\lambda_\omega|^2$, is a result of the plasma process that must produce

the “clumps”, and is unknown. It is likely to be cut off above some frequency ω_p , perhaps an electron plasma frequency. A process that accelerates electrons also accelerates positrons in the opposite direction, naturally leading to two-stream instability with frequencies close to the electron plasma frequency (Lu & Kumar 2018).

If $\omega_p \gg \omega_c$ then the radiated spectrum $P(\omega)$ will be cut off exponentially by $E_{point,\omega}$ for $\omega > \omega_c$ and will be modulated by $|\lambda(\omega)|^2$ for $\omega < \omega_c$. If $\omega_p \ll \omega_c$ the radiation spectrum will be $\propto \omega^{1/3} |\lambda_\omega|^2$. This is essentially the spectrum of the charge density passing the point on the arc ($\theta = 0$) at which the motion is most closely directed towards the observer. The emitted radiation has the spectrum of the plasma turbulence multiplied by the intrinsic spectrum $E_{q,\omega}$ of curvature radiation by a point particle. Because the latter spectrum is so broad and smooth, at frequencies less than the characteristic curvature radiation frequency their product is close to the spectrum of the turbulence. It is then not possible to infer γ from the observed frequency ω_{obs} except to set a lower bound from the condition that $\omega_{obs} \lesssim \omega_p \ll \omega_c$:

$$\gamma \gtrsim \left(\frac{\omega_{obs} \rho}{c} \right)^{1/3} \approx 50 \quad (5)$$

for neutron star parameters and the observation (Gajjar *et al.* 2018) of FRB 121102 at $\nu = 8$ GHz. For FRB observed at 1.2–1.5 GHz the corresponding lower bound is $\gamma \gtrsim 30$. Without an understanding of the plasma turbulence, it is not possible to predict to how high frequencies FRB produce observable coherent radiation.

3.2 The Clump Charge

It is possible to estimate the coherently moving charges Q required to explain the observed FRB. Using Eq. 1 (Kumar, Lu & Bhattacharya 2017), the maximum electric field at the observer is obtained by taking $\alpha = 0$ and $\theta = 0$:

$$E_{max} = \frac{Q\beta^2}{d\rho} \left[\frac{1-\beta}{(1-\beta)^3} \right] \approx \frac{Q}{d\rho} \frac{1}{(1-\beta)^2} \approx \frac{4Q\gamma^4}{d\rho}, \quad (6)$$

where we take $\gamma \gg 1$. Fields comparable to this value are radiated into a solid angle $\sim \gamma^{-2}$ at the source.

An isotropically radiating source of radius R will have $\sim R^2/[\gamma^2(\lambda/2)^2]$ independently radiating emitters producing fields $\sim E_{max}$ at the observer, provided $\gamma < 2R/\lambda$. These emitters combine incoherently, and their intensities add. Then, using

$$I = \frac{R^2}{\gamma^2(\lambda/2)^2} \frac{c}{8\pi} E_{max}^2 \quad (7)$$

and taking $R \sim \rho$, as expected for a dipole field,

$$Q \sim \sqrt{\frac{\pi I \lambda d}{8c}} \frac{1}{\gamma^3} \sim \sqrt{\frac{I}{\text{Jy-GHz}}} \frac{\lambda}{20 \text{ cm}} \frac{d}{1 \text{ Gpc}} \frac{1}{\gamma^3} 2 \times 10^{16} \text{ esu.} \quad (8)$$

If $\gamma \sim 60$, as required for $\omega_c = 2\pi \times 1.4$ GHz curvature radiation from a neutron star magnetosphere, and $I \sim 1$ Jy-GHz, a nominal FRB value, then $Q \sim 10^{11}$ esu ~ 30 Coulombs. This value of γ is only a rough lower bound (Kumar, Lu & Bhattacharya (2017) consider $\gamma \sim 30$). If γ is higher the required Q is less; then Eq. 6 must be replaced by a more complex expression (Jackson 1999). Although the observation of radiation at some frequency ω places a lower

bound on γ , it may exceed this lower bound by a large factor (if $\omega \ll \omega_c$), so that Eq. 8 cannot, without independent information about γ , be interpreted as placing a lower bound on Q .

These results also apply to observers illuminated by a collimated source (Katz 2017a,c). Collimation reduces the total radiated power, but does not change the required Q .

3.3 Characteristic Lorentz Factor and Frequency

Taking $\gamma^3 = 2\omega_c \rho / (3c) = (4\pi/3)\rho/\lambda$ and $\rho \sim 10^6$ cm and substituting in Eq. 8:

$$Q \sim \sqrt{\frac{I}{\text{Jy-GHz}}} \left(\frac{\lambda}{20 \text{ cm}} \right)^2 \frac{d}{1 \text{ Gpc}} 4 \times 10^{10} \text{ esu,} \quad (9)$$

Qualitatively, higher frequency radiation may make less severe demands on Q .

The existence of large coherent charge clumps (Eq. 8) implies, if the charge is distributed over a region of size $\sim \lambda/2$, large electrostatic potentials

$$V \sim \frac{Q}{(\lambda/2)} \sim \sqrt{\frac{\pi I}{2c}} \frac{d}{\gamma^3}. \quad (10)$$

This suggests a minimum or characteristic Lorentz factor γ_c set by equating the electron or positron energy $\gamma_c m_e c^2$ to its electrostatic energy eV . Then

$$\begin{aligned} \gamma_c &= \left(\frac{\pi I}{2c} \right)^{1/8} \left(\frac{ed}{m_e c^2} \right)^{1/4} \\ &\sim \left(\frac{I}{\text{Jy-GHz}} \right)^{1/8} \left(\frac{d}{\text{Gpc}} \right)^{1/4} 1.1 \times 10^3. \end{aligned} \quad (11)$$

Defining an equivalent isotropic radiated power $P_{eq} \equiv 4\pi I d^2$, this may be rewritten

$$\gamma_c = \left(\frac{P_{eq}}{8\pi m_e^2 c^5 / e^2} \right)^{1/8} \approx 1000 \left(\frac{P_{eq}}{10^{42} \text{ erg/s}} \right)^{1/8}. \quad (12)$$

The fields of collimated relativistic particles moving towards the observer add coherently if they are distributed over a distance along their path $\sim \gamma^2 \lambda/2$. Then Eqs. 10–12 are replaced by

$$V \sim \frac{Q}{(\lambda/2)\gamma^2} \sim \sqrt{\frac{\pi I}{2c}} \frac{d}{\gamma^5}. \quad (13)$$

Again equating $\gamma_c m_e c^2 = eV$,

$$\begin{aligned} \gamma_c &= \left(\frac{\pi I}{2c} \right)^{1/12} \left(\frac{ed}{m_e c^2} \right)^{1/6} \\ &\sim \left(\frac{I}{\text{Jy-GHz}} \right)^{1/12} \left(\frac{d}{\text{Gpc}} \right)^{1/6} 1.0 \times 10^2 \end{aligned} \quad (14)$$

and

$$\gamma_c = \left(\frac{P_{eq}}{8\pi m_e^2 c^5 / e^2} \right)^{1/12} \approx 100 \left(\frac{P_{eq}}{10^{42} \text{ erg/s}} \right)^{1/12}. \quad (15)$$

These estimates of γ_c are more general than that of Eq. 5 that refers specifically to curvature radiation in inner neutron star magnetospheres.

These results apply to any radiation process in which coherent charge bunches are accelerated perpendicular to their velocity, and even if the radiation is collimated and the actual radiated power is much less than P_{eq} . Note that

it is possible that the Lorentz factor of the radiating charges $\gamma \gg \gamma_c$; γ_c is only the minimum implied by the existence of large electrostatic potentials in the source.

The characteristic Lorentz factor of Eq. 11 implies a characteristic frequency of curvature radiation $\omega_c = 3\gamma_c^3 c/2\rho$:

$$\omega_c \sim \left(\frac{I}{\text{Jy-GHz}}\right)^{3/8} \left(\frac{d}{\text{Gpc}}\right)^{3/4} \left(\frac{10^6 \text{ cm}}{\rho}\right) 5 \times 10^{13} \text{ s}^{-1}, \quad (16)$$

while Eq. 14 implies

$$\omega_c \sim \left(\frac{I}{\text{Jy-GHz}}\right)^{1/4} \left(\frac{d}{\text{Gpc}}\right)^{1/2} \left(\frac{10^6 \text{ cm}}{\rho}\right) 5 \times 10^{10} \text{ s}^{-1}, \quad (17)$$

If the factors in parentheses are ~ 1 , as for a FRB produced in a neutron star magnetosphere at cosmological distances, Eq. 16 corresponds to infrared radiation with $\lambda \sim 30 \mu$ while Eq. 17 corresponds to $\nu \sim 10$ GHz, approximately the highest frequency at which FRB have been observed. For there to be coherent radiation at these frequencies, the structure factor λ_ω of the charge distribution must be significant for $\omega \sim \omega_c$. The underlying plasma physics is complex and likely not understood, and there is no *a priori* reason to expect observable coherent radiation. Despite this, because γ_c is only a lower bound curvature radiation at yet higher frequencies than those of Eqs. 16 and 17 is possible.

4 DISCUSSION

The classical spectrum of curvature or synchrotron radiation (Jackson 1999) is that radiated by point charges. Coherent emission requires a large number of charges spread over a finite region; electrostatic repulsion spreads out “clumps” of charge that cannot be treated as points. They must be described by continuous distributions of charge density, which also imply continuous distributions of the times they pass the small (for relativistic particles) region producing significant fields at the observer.

Only the insignificant incoherent part of the emission is described by the classical result $E_{point,\omega}$ for the radiated field of point charges. Very little power may be emitted at frequencies around the classical characteristic frequency ω_c of incoherent curvature radiation. The Lorentz factors of radiating particles cannot then be inferred from the frequency of the observed radiation and may be much higher. Observed spectral cutoffs are likely to reflect the spatial distribution of the charge density, not the characteristic frequency of curvature radiation.

The coherently radiated field reflects the distribution and motion of the smoothed charge density, a continuous function of the coordinates. The radiation mechanism may be described as hybrid coherent plasma-curvature radiation. This resolves the disagreement between the physically plausible mechanism of curvature radiation and the apparently inconsistent observed spectrum.

The results of Eqs. 11–16 are very generally applicable to coherent nonthermal sources of high brightness emission, not only FRB, and do not depend on the emission mechanism.

ACKNOWLEDGEMENTS

I thank C. J. Law for providing the raw data for Fig. 1 and V. Gajjar, P. Kumar, C. J. Law, W. Lu and V. Ravi for useful discussions.

REFERENCES

- Bannister, K. W., Shannon, R. M., Macquart, J.-P. *et al.* 2017 ApJ 841, L12.
- Burke-Spolaor, S. & Bannister, K. W. 2014 ApJ 792, 19.
- Chatterjee, S., Law, C. J., Wharton, R. S. *et al.* 2017 Nature 541, 58.
- Cordes, J. M. & Lazio, T. J. W. 2002 arXiv:astro-ph/0207156.
- Cordes, J. M., Wasserman, I., Hessels, J. W. T. *et al.* 2017 ApJ 842, 35.
- Dai, Z. G., Wang, J. S., Wu, X. F. *et al.* 2016 ApJ 829, 27.
- Farah, W., Flynn, C., Bailes, M. *et al.* 2018 MNRAS 478, 1209 arXiv:1803.05697.
- Gajjar, V., Siemion, A. P. V., MacMahon, D. H. E. *et al.* 2018 ApJ 863, 2 arXiv:1804.04101.
- Ghisellini, G. & Locatelli, N. 2018 A&A 613, 61 arXiv:1708.07507.
- Gu, W.-M., Dong, Y.-Z., Liu, T. *et al.* 2016 ApJ 823, L28.
- Hankins, T. H. & Eilek, J. A. 2007 ApJ 670, 693.
- Hardy, L. K., Dhillon, V. S., Spitler, L. G. *et al.* 2017 MNRAS 472, 2800.
- Jackson, J. D. 1999 Classical Electrodynamics (3rd ed.) Chichester: Wiley.
- Katz, J. I. 2014 Phys. Rev. D 89, 103009.
- Katz, J. I. 2016 Mod. Phys. Lett. A 31, 1630013.
- Katz, J. I. 2017a MNRAS 467, L96.
- Katz, J. I. 2017b MNRAS 469, L39.
- Katz, J. I. 2017c MNRAS 471, L92.
- Keane, E. F., Stappers, B. W., Kramer, M. *et al.* 2012 MNRAS 425, L71.
- Kumar, P., Lu, W. & Bhattacharya, M. 2017 MNRAS 468, 2726.
- Law, C. J., Abruzzo, M. W., Bassa, C. G. *et al.* 2017 ApJ 850, 76.
- Lorimer, D. R., Bailes, M., McLaughlin, M. A., Narkevic, D. J. & Crawford, F. 2007 Science 318, 777.
- Lu, W. & Kumar, P. 2018 MNRAS 477, 2470 arXiv:1710.10270.
- Marcote, B., Paragi, Z., Hessels, J. W. T. *et al.* 2017 ApJ 834, L8.
- Masui, K., Lin, H.-H., Sievers, J. *et al.* 2015 Nature 528, 523.
- Melrose, D. B. 2017 Rev. Mod. Plasma Phys. 1:5 doi.org/10.1007/s41614-107-0007-0.
- Michilli, D., Seymour, A., Hessels, J. W. T. *et al.* 2018 Nature 553, 182.
- Oostrum, L. C., van Leeuwen, J., Attema, J. *et al.* 2017 ATel. 10693.
- Petroff, E., Bailes, M., Barr, E. D. *et al.* MNRAS 447, 246.
- Petroff, E., Barr, E. D., Jameson, A. *et al.* FRBCAT: The Fast Radio Burst Catalogue 2016 Pub. Ast. Soc. Aust. 33, id.e045 <http://www.frbcat.org> downloaded March 25, 2018.
- Petroff, E., Burke-Spolaor, S., Keane, E. F. *et al.* 2017 MNRAS 469, 4465.
- Ravi, V., Shannon, R. M. & Jameson, A. 2015 ApJ 799, L5.
- Ravi, V., Shannon, R. M., Bailes, M. *et al.* 2016 Science 354, 1249; supplementary material in arXiv:1611.05758.
- Rickett, B. J. 1990 ARA&A 28, 561.
- Scholz, P., Spitler, L. G., Hessels, J. W. T. *et al.* 2016 ApJ 833, 177.
- Soglasnov, V. A., Popov, M. V., Bartel, N., Cannon, W., Novikov, A. Y., Kondratiev, V. I. & Altunin, V. I. 2004 ApJ 616, 439.
- Spitler, L. G., Cordes, J. M., Hessels, J. W. T. *et al.* 2014 ApJ 790, 101.
- Spitler, L. G., Scholz, P., Hessels, J. W. T. *et al.* 2016 Nature 531, 202.

Thornton, D, Stappers, B., Bailes, M. *et al.* 2013 *Science* 341, 53.
Wang, J.-S., Yang, Y.-P., Wu, X.-F. *et al.* 2016 *ApJ* 822, L7.
Yang, Y.-P. & Zhang, B. 2017 arXiv:1712.02702.

This paper has been typeset from a $\text{\TeX}/\text{\LaTeX}$ file prepared by the author.